Rheol. Acta **19**, 19 – 31 (1980)

ISSN 0035-4511 / ASTM-Coden: RHEAAK

Department of Aerospace Engineering and Mechanics
University of Minnesota, Minneapolis, Minnesota

The free surface on a liquid between cylinders rotating at different speeds. Part III

G. S. Beavers, J. Y. Yoo and *D. D. Joseph*

With 12 figures and 1 table

(Received March 29, 1979)

1. Introduction

When a viscoelastic fluid is sheared between two concentric cylinders undergoing differential rotation the free surface on the fluid is deformed as a consequence of the normal stresses induced in the fluid by the shearing motion. This free surface deformation in the concentric cylinder geometry is the general Weissenberg effect. If the radius of the inner cylinder is small compared with that of the outer cylinder the normal stresses will drive the fluid up the inner cylinder provided that the radius of the inner cylinder is less than a critical value which depends upon some of the parameters which characterize the fluid. However, when the radii of the two cylinders are comparable, the response of the free surface to the normal stresses is not simple, and the free surface can exhibit a variety of shapes which depend not only upon the viscoelastic parameters characterizing the fluid but also upon the radii of the cylinders and the differential rotation speed.

In a series of papers concerned with the Weissenberg effect we have promoted the concept of using measurements of the deformed free surface to provide information about the constitutive equation for the fluid. The application of domain perturbation analysis to the Weissenberg geometry has been discussed in an earlier review paper by *Joseph* and *Beavers* (1), where it is shown how a mathematical description of the Weissenberg effect can be obtained in a series of powers of the angular speed Ω of the inner cylinder. The equations which govern the perturbation fields were first derived in the paper by *Joseph* and *Fosdick* (2), which forms the starting point of our work in this area. In that paper, however, the important contribution of surface tension is not included at orders higher than second, and at second order it is only included in the problem of the flow induced by a rotating cylinder in an infinite fluid and not in the more general problem of the flow between cylinders. *Joseph, Beavers* and *Fosdick* (3) showed how experiments on free surfaces induced by the steady rotation of cylinders of small diameter in a large volume of fluid can be used with the second-order theory to yield rheological data for the fluid. A much more extensive experimental program involving the same geometry was reported by *Beavers* and *Joseph* (4), in which we showed that the polymeric oils used for our experiments have a second-order range, that is a range in which the height of climb is linear in Ω^2. In the second-order theory there is only one viscoelastic parameter; and it was shown in (4) that the values of this parameter, and its dependence on temperature, could be determined from measurements of the height of climb at the rotating cylinder.

Up to this point in our research we had confined our experiments to cylinders of small diameter rotating in large volumes of fluid, because the complete perturbation solutions were available for this geometry. Recently we have completed the perturbation analysis up to and including terms of $0(\Omega^4)$ for the concentric cylinder geometry (*Yoo, Joseph* and *Beavers* (5)). The analysis shows that the response of any viscoelastic fluid to steady rotation of the cylinders through terms of $0(\Omega^4)$ depends on the viscosity and on four viscoelastic parameters. All five parameters can be determined from measurements of quantities computed in the theory, and in (5) we outline the procedure for doing this. One of the parameters is determined

from measurements of the circumferential component of velocity on the free surface of the fluid. To investigate the feasibility of the whole procedure we measured circumferential velocity profiles for rods of small diameter rotating in large volumes of three different viscoelastic fluids, and obtained excellent agreement with the predictions of analysis.

This paper is a further contribution to our work on the Weissenberg effect, and presents a second experimental test of the analysis of ref. (5). We report the results from a comprehensive series of experiments in which free surface profiles were measured on three different fluids sheared in a concentric cylinder apparatus consisting of a fixed outer cylinder and four interchangeable inner cylinders. The experimental profiles are compared with the profiles predicted from second-order theory, and the limitations of the second-order theory as revealed by these comparisons are discussed.

2. Second-order theory

The complete perturbation analysis for the concentric cylinder geometry has been completed through fourth order (*Yoo, Joseph* and *Beavers* (5)). The procedures required by the fourth-order theory for the determination of the values of the viscoelastic parameters through order four are much more elaborate and probably less accurate than those used in the second-order theory. In this paper we restrict our calculations to second-order results, and compare experimentally-measured free surface shapes with those predicted from the second-order theory. This has the advantage that at second order only one viscoelastic parameter, namely the climbing constant, enters the solutions, and this parameter can be determined independently from experiments with small diameter rods undergoing steady rotation in large volumes of fluid. We shall not repeat here all the details of the second-order theory, but merely outline the principal features of the theory and quote the results which are essential to the presentation of the experimental data and the comparison of the data with the predictions of the analysis.

An incompressible viscoelastic fluid is set into axisymmetric motion between two concentric cylinders. The outer cylinder ($r = b$) is at rest and the inner cylinder ($r = a$) rotates with a steady angular velocity Ω. The free surface on top of the fluid deforms into an axisymmetric shape given by $z = h(r;\Omega)$, which was flat when $\Omega = 0$. The region occupied by the fluid is designated as

$$\mathscr{V}_\Omega = \{r,\theta,z \mid a \le r \le b,\ 0 \le \theta \le 2\pi,\ -\infty < z \le h(r;\Omega)\}$$

where (r,θ,z) are cylindrical coordinates. In $\mathscr{V}_\Omega$ we have

$$\rho(\boldsymbol{u}\cdot\nabla)\boldsymbol{u} = -\nabla\Phi + \nabla\cdot\boldsymbol{S}, \qquad [1.1]$$

$$\nabla\cdot\boldsymbol{u} = 0 \qquad [1.2]$$

where $\Phi(r,z) = p(r,z) - p_a + \rho g z$, p is the constitutively indeterminate pressure, p_a is local atmospheric pressure, and $\boldsymbol{S}$ is the extra stress. The boundary conditions are

$$\boldsymbol{u} = \begin{cases} e_\theta \Omega a & \text{at} \quad r = a \\ 0 & \text{at} \quad r = b \end{cases} \qquad [2]$$

and on the free surface of the fluid domain the shear traction vector and the normal component of the velocity vanish:

$$\boldsymbol{u}\cdot\boldsymbol{n} = S_{n\theta} = S_{nt} = 0 \quad \text{at} \quad z = h(r;\Omega) \qquad [3]$$

where $\boldsymbol{n}$ is the outward unit normal to the free surface and $\boldsymbol{t}$ is the unit tangent vector in the intersection of the free surface and the plane θ = constant.

Across the free surface the jump in normal stress is balanced by the surface tension T. Thus at $z = h(r;\Omega)$

$$\rho g h - \Phi + S_{nn} - \frac{T}{r}\left(\frac{rh'}{(1+(h')^2)^{1/2}}\right)' = 0, \qquad [4]$$

which is to be solved subject to one of the following pairs of boundary conditions:

$$\frac{dh(a;\Omega)}{dr} = \frac{dh(b;\Omega)}{dr} = 0, \qquad [5.1]$$

$$h(a;\Omega) = h(b;\Omega) = 0, \qquad [5.2]$$

$$\frac{dh(a;\Omega)}{dr} = h(b;\Omega) = 0, \qquad [5.3]$$

$$h(a;\Omega) = \frac{dh(b;\Omega)}{dr} = 0. \qquad [5.4]$$

We also make use of the condition that the total volume below the free surface is conserved:

$$\int_a^b r h(r;\Omega)\,dr = 0. \qquad [6]$$

This makes Φ definite and fixes the plane on which $z = 0$.

The extra stress $\boldsymbol{S}$ is expanded into a Taylor series whose partial sum is

$$\boldsymbol{S}_{(N)} = \sum_{n=1}^{N} \boldsymbol{S}_n [\boldsymbol{A}_n, \boldsymbol{A}_{n-1}, \ldots, \boldsymbol{A}_1]$$

where the $\boldsymbol{A}_n$ are Rivlin-Ericksen kinematic tensors. At second order only the first two of the $\boldsymbol{S}_n$ are required:

$$\boldsymbol{S}_1 [\boldsymbol{A}_1] = \mu \boldsymbol{A}_1 , \qquad [7.1]$$

$$\boldsymbol{S}_2 [\boldsymbol{A}_1, \boldsymbol{A}_2] = \alpha_1 \boldsymbol{A}_2 + \alpha_2 \boldsymbol{A}_1^2 \qquad [7.2]$$

where the coefficients μ, α_1 and α_2 are functions of temperature (4).

A formal solution is obtained as a series in powers of Ω whose coefficients are derivatives of the solution evaluated at the rest state. For example, we write

$$h(r\,;\Omega) = \tfrac{1}{2}\Omega^2 h^{[2]}(r_0) + 0(\Omega^4) \qquad [8]$$

where (r_0, z_0) are coordinates of the rest state defined in

$$\mathscr{V}_0 = \{r_0, \theta_0, z_0 \mid a \le r_0 \le b,\ 0 \le \theta_0 \le 2\pi,\ -\infty < z_0 \le 0\},$$

and $h^{[2]}(r_0)$ is a substantial derivative taken with respect to Ω at $\Omega = 0$ when r_0 and z_0 are fixed. The coordinates (r_0, z_0) are related to (r, z) by an invertible shifting transformation

$$r = r_0 , \quad \theta = \theta_0 , \quad z = z_0 + h(r_0\,;\Omega)$$

which maps boundary points $z = h$ in $\mathscr{V}_\Omega$ into boundary points in $\mathscr{V}_0$.

Details of the analytical steps leading from [4] to the final equation for $h^{[2]}$ are given in ref. (5). The equation is

$$\frac{T}{r_0}\frac{d}{dr_0}\left(r_0 \frac{dh^{[2]}}{dr_0}\right) - \rho g h^{[2]} + \Phi^{\langle 2\rangle} = 0 \quad \text{at} \quad z = 0 \qquad [9]$$

where $h^{[2]}$ satisfies one of the pairs of boundary conditions [5.1]–[5.4] expressed in terms of $h^{[2]}$. The derivative $\Phi^{\langle 2\rangle}$ appearing in eq. [9] is the derivative of the total head Φ taken with respect to Ω at $\Omega = 0$ when r and z are fixed. An explicit expression for $\Phi^{\langle 2\rangle}$ can be found involving the radii a and b, the surface tension T, and the climbing constant $\hat{\beta} = 3\alpha_1 + 2\alpha_2$, (5).

It is convenient for computational purposes to work in terms of dimensionless quantities. To do this we introduce the following dimensionless quantities:

$$t = \frac{2r_0}{b-a}, \qquad \eta = \frac{a}{b},$$

$$\hat{S} = \frac{\rho g b^2 (1-\eta^2)}{4T}, \qquad \hat{R} = \frac{4\hat{\beta}}{\rho b^2 \eta^2}.$$

The derivatives $h^{[2]}$ and $\Phi^{\langle 2\rangle}$ may then be written in the form

$$\frac{g h^{[2]}(r_0)}{b^2\eta^2} = H_{21}(t) + \hat{R} H_{22}(t), \qquad [10]$$

$$\frac{\Phi^{\langle 2\rangle}(r_0)}{\rho b^2 \eta^2} = \Phi_{21}(t) + \hat{R}\Phi_{22}(t). \qquad [11]$$

In writing eqs. [10] and [11] we have used the principle of superposition to reduce the solution to the computation of functions of η and $\hat{S}$ alone. For fixed values of the group $\rho g/T$, the prescription of η and $\hat{S}$ is equivalent to prescribing the radii of the inner and outer cylinders. Hence when $\rho g/T$ is fixed the dimensionless functions are independent of material parameters.

The height rise functions in eq. [10] satisfy

$$\frac{1}{t}\frac{d}{dt}\left(t\frac{dH_{2i}}{dt}\right) - \hat{S}H_{2i} + \hat{S}\Phi_{2i}(t) = 0, \quad i = 1,2 \qquad [12]$$

and one pair of the four possible boundary conditions [5.1]–[5.4]. The functions $\Phi_{21}(t,\eta)$ and $\Phi_{22}(t,\eta)$ can be found explicitly:

$$\Phi_{21}(t,\eta) = \frac{\eta^2}{(1-\eta^2)^2}\left((1-\eta)^2 t^2 - 4\ln\frac{(1-\eta)t}{2\eta} - \frac{4}{(1-\eta)^2 t^2}\right) - \frac{6\eta^2 \ln\eta}{(1-\eta^2)^3} - \frac{2\eta^2(2+\eta^2)}{(1-\eta^2)^2} - \frac{1}{2\hat{S}(1+\eta)^2}\left(t\frac{dH_{21}}{dt}\right)\Bigg|_a^b, \qquad [13]$$

$$\Phi_{22}(t,\eta) = \frac{16\eta^4}{(1-\eta^2)^2(1-\eta^4)t^4} - \frac{\eta^2}{(1-\eta^2)^2} - \frac{1}{2\hat{S}(1+\eta)^2}\left(t\frac{dH_{22}}{dt}\right)\Bigg|_a^b. \qquad [14]$$

Thus, when $\hat{S}$ and η are given, eq. [12] can be solved numerically using the appropriate bound-

ary conditions to yield the shape of the free surface of the fluid.

3. Experiments

3.1. Apparatus

The central part of the apparatus consisted of a stationary outer cylinder and four interchangeable inner cylinders. The construction of the cylinders is illustrated in figure 1.

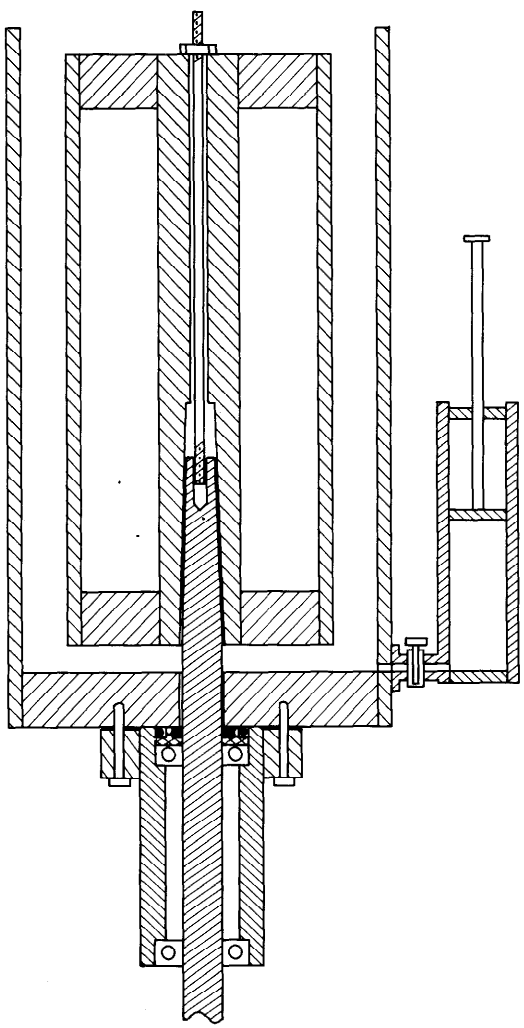

Fig. 1. Schematic of the concentric cylinder apparatus, illustrating the construction of the cylinders

The outer cylinder was made of aluminum, with a wall thickness of 0.64 cm, a 2.54 cm bottom plate, an inside depth of 30.4 cm and an inside radius of 8.588 cm. The three largest inner cylinders were made from hollow aluminum tubes, with a wall thickness of 0.64 cm. The radii of the inner cylinders were 3.936, 5.018, 5.704 and 6.477 cm, and each cylinder was 27.95 cm long. An aluminum central core, 3.81 cm in diameter, was built into each cylinder, and a number-two Morse taper was machined into the core. This female taper mated with a similar taper on the end of the drive shaft. The inner cylinder was locked securely in place on the drive shaft by means of a long threaded bolt which passed through the central core and screwed into the end of the shaft. The drive shaft passed through a housing containing seals and bearings, and which was attached to the underside of the bottom plate of the stationary cylinder. Accurate alignment of the drive shaft was maintained by means of the bearings in the housing and two other bearings located on the rigid aluminum frame to which the equipment was attached.

A small reservoir was attached to the outer cylinder and connected to the lowest point of the inter-cylinder space through a shut-off valve. The reservoir was equipped with a plunger which was used between experimental runs to inject small amounts of fluid into the main body of fluid. This allowed the level of the undisturbed free surface of the fluid to be adjusted so that if the fluid climbed at either cylinder wall it would climb on to a dry, uncoated surface. The reservoir system was also useful in the initial filling and the final draining operations.

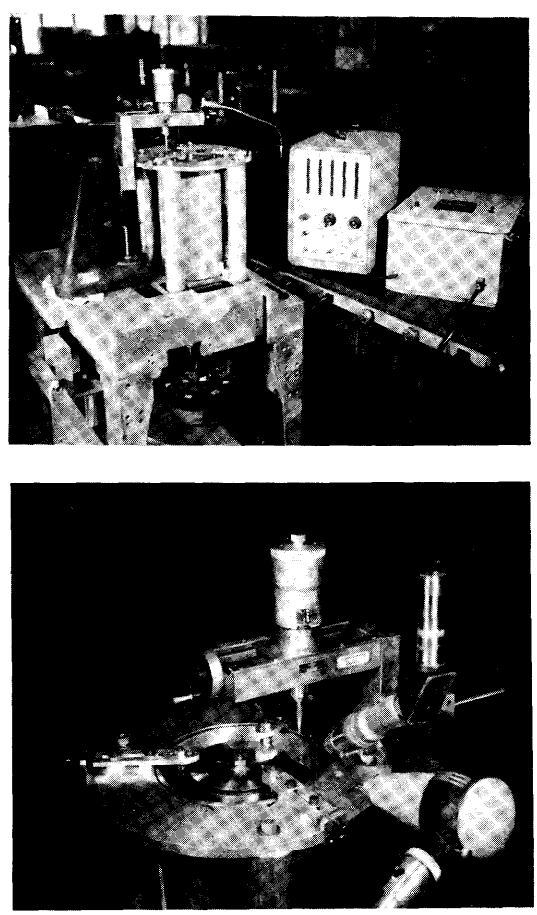

Fig. 2. The experimental equipment and the system used for measuring the free-surface profiles

The method of attachment of the inner cylinder assured concentricity at the lower end. Concentricity was maintained at the upper end by means of three equally-spaced roller bearings which pressed against the inner cylinder. The radial position of each bearing was adjusted by means of a fine-threaded screw. The bearings were mounted on a rigid platform which was supported by four posts rigidly attached to the main frame. The only contact between this part of the apparatus and the concentric cylinders was through the three bearings at the inner cylinder. The components of the apparatus can be clearly identified in the two photographs of figure 2.

The concentricity of the cylinders was set and checked during the initial installation of an inner cylinder by means of a specially designed gauge, illustrated in the upper part of figure 3 and shown in use in the lower part of that figure. The gauge consists essentially of a cantilever beam fitted with a strain gauge. Teflon posts and interchangeable teflon legs allow the gauge to make the equivalent of three-point contact with the cylinders, and to be moved to any azimuthal location at any depth in the gap between the cylinders. Variations of 0.0001 cm in the dimension of the gap could be detected with this device. During an experiment the variation in the gap dimension was no worse than 0.002 cm*).

The inner cylinder was driven by an Electrocraft Motomatic Type E-710 d.c. servo-motor with a feedback control system. A timing-belt drive was used between the motor and the drive-shaft for the inner cylinder, giving a speed reduction of 5.25 to 1. Rotational speeds were measured by means of a light source and photomultiplier tube connected to a digital counter, and ten reflecting surfaces on the motor drive shaft.

Surface profiles were measured by observing a sharp needle and its reflection in the fluid surface through a measuring microscope. The needle was attached to a micrometer, which in turn was mounted on a microscope traversing mechanism. The whole traversing system was attached to a massive base and accurately aligned for movement in the radial direction (fig. 2).

Experiments were carried out with three different fluids: TLA-227, a methacrylate copolymer in oil, manufactured by the Texaco Oil Company; STP oil additive, a solution of polyisobutylene in oil; and a 2.0% by weight solution of polyacrylamide (Cyanamid P 250 manufactured by the American Cyanamid Company) in a 49% water – 49% glycerin solvent. All four inner cylinders were used with all three fluids,

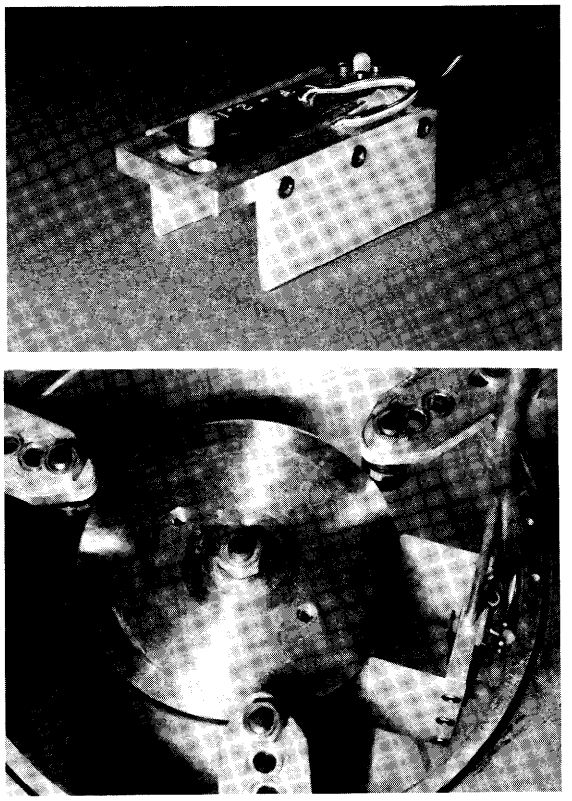

Fig. 3. The gauge used for checking the concentricity of the cylinders

at five different rotational speeds in both the clockwise and counterclockwise directions.

3.2. Experiments with TLA-227

The first step in the experimental program with each fluid was the determination of the climbing constant $\hat{\beta} = 3\alpha_1 + 2\alpha_2$. This was accomplished using the technique described in ref. (4). The data from which $\hat{\beta}$ for TLA-227 was calculated are shown in the lower half of figure 4. Two cylinders, with radii of 0.953 and 0.631 cm, were used and the height of climb h at the rod was measured as a function of rod rotational speed ω. The climbing constant was then computed from the second order solution for a rod in an infinite fluid (4):

$$\frac{dh}{d\omega^2} = \frac{2\pi^2 a}{TS^{1/2}}\left(\frac{4\hat{\beta}}{4+\lambda} - \frac{\rho a^2}{2+\lambda}\right)$$

where $\lambda^2 = a^2 S$ and $S = \rho g/T$. The average value of $\hat{\beta}$ for TLA-227 determined from the data of figure 4 was 29.0 gram cm^{-1}. The density ρ and surface tension T were determined by

*) *Note added in proof:* It is important to remark that in the case of eccentric cylinders the solution is not even in Ω. The eccentricity produces a lubrication effect which is odd in Ω, which is independent of normal stresses, and which dominates the dynamics when Ω is small. That is why our experimental results depend critically on careful alignment of the cylinders and why the 'rotating rod' is more useful for rheological measurements.

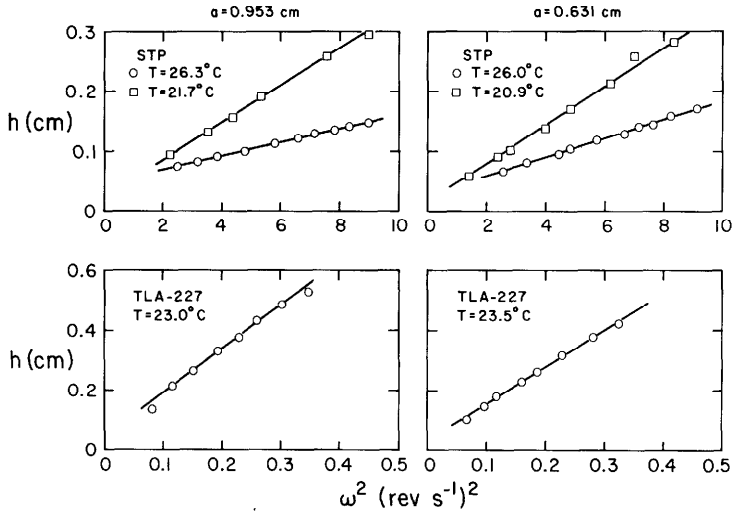

Fig. 4. The data from which the climbing constants for STP and TLA-227 were determined: the height of climb at the rod surface for a circular rod rotating in a large volume of fluid. The rotational speeds are restricted to the second-order range

standard methods and found to be $\rho = 0.896$ gram cm^{-3} and $T = 30.9$ dynes cm^{-1}.

Theoretically-predicted free surface profiles for this sample of TLA-227 are shown in figure 5 for the four inner cylinders which were employed in our experiments and for four smaller inner cylinders. The profiles are those corresponding to a rotational speed of 0.16 rev/sec. Two profiles are shown for each inner cylinder, one associated with the zero slope boundary conditions at both the inner and outer walls, and the second associated with the zero slope boundary condition at the inner cylinder and a fixed point of attachment at the outer cylinder. The climbing constant for TLA-227 is large, and the predicted profiles are those which we would anticipate from the Weissenberg effect, with the fluid climbing up the inner cylinder and being depressed near the outer cylinder. It is clear from figure 5 that the boundary condition at the outer

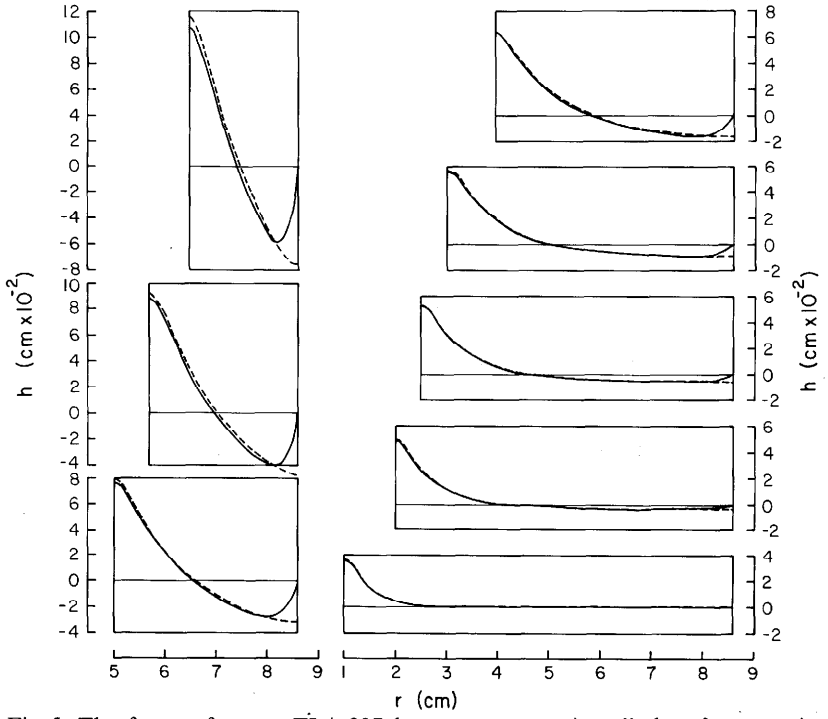

Fig. 5. The free surface on TLA-227 between concentric cylinders for a stationary outer cylinder of radius 8.588 cm and various inner cylinders rotating at 0.16 rev s^{-1}: – – –, zero slope boundary condition at both walls; ———, fixed point of attachment at the outer cylinder

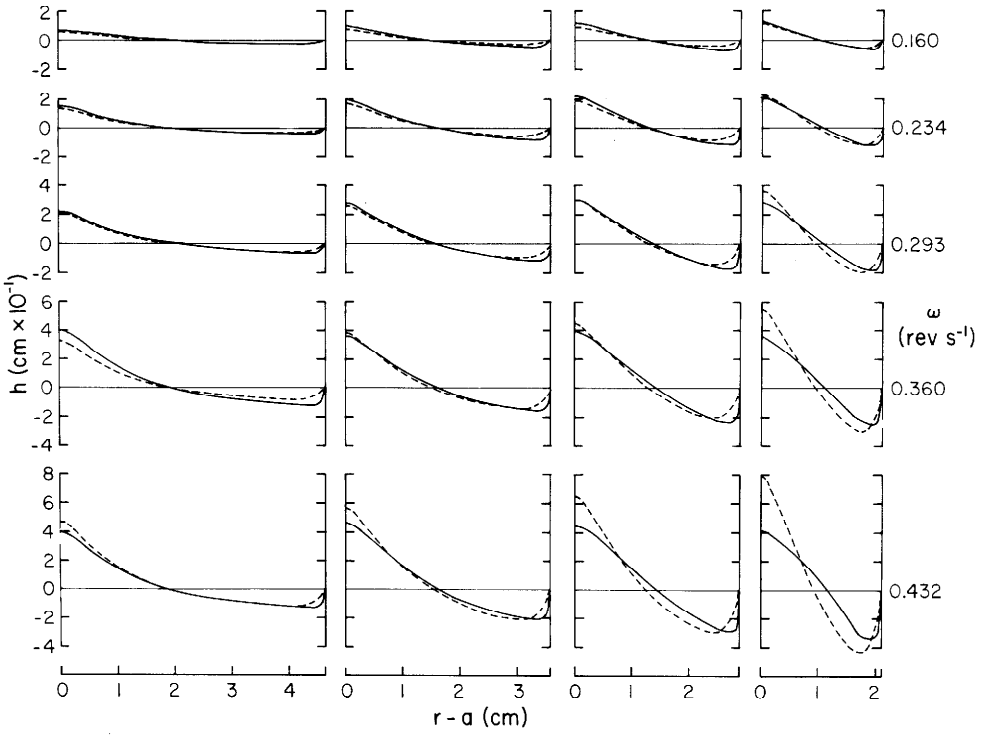

Fig. 6. Experimental (———) and predicted (– – –) profiles for TLA-227 at five different rotational speeds of the inner cylinder. The radius of the outer cylinder is 8.588 cm, and the radii of the four inner cylinders are 3.936, 5.018, 5.704 and 6.477 cm

cylinder has little effect on the shape of the climbing fluid except for small clearances between the two cylinders.

Comparisons of experimentally-measured profiles with predicted profiles are presented in figure 6 for the four inner cylinders operating at five different rotational speeds. The temperature of the fluid throughout all the experiments was between 23 °C and 24 °C. Although we did not monitor the temperature continuously during a traverse across the surface, we did measure it immediately before and immediately after each traverse by inserting a thermocouple into the fluid at different depths.

In computing the predicted profiles for figure 6 we have used the fixed contact line boundary condition at the outer cylinder wall where the fluid is depressed. We have observed in past experiments with fluids of the type used for these experiments that once a surface has been wetted with the fluid there always remains a thin coating of the fluid on the surface. For this reason the appropriate boundary condition at the outer cylinder is the fixed contact line condition. It appears from figure 6, however, that the analysis predicts a somewhat thicker layer of fluid on the outer cylinder than observed in the experiments. The agreement between measured and predicted profiles is good at the lower angular velocities, and gets progressively worse as the angular velocity is increased, when effects of higher order than second begin to dominate. Also, as the gap between the cylinders is made small, the higher order effects become important at lower angular speeds. We will comment further on this in § 3.5.

Our apparatus was constructed so that the inner cylinder could be rotated in either direction, and we used this feature to provide a check on the accuracy of our measurements. After each series of traverses we repeated the experiment with the cylinder rotating in the opposite direction. Two groups of surface profiles measured for clockwise and counterclockwise rotations are illustrated in figure 7. The comparisons for the larger gap are typical of almost all our measurements, whereas the comparisons for the smaller gap represent the worst case. We believe that a major source of the discrepancy between the two profiles for the smaller

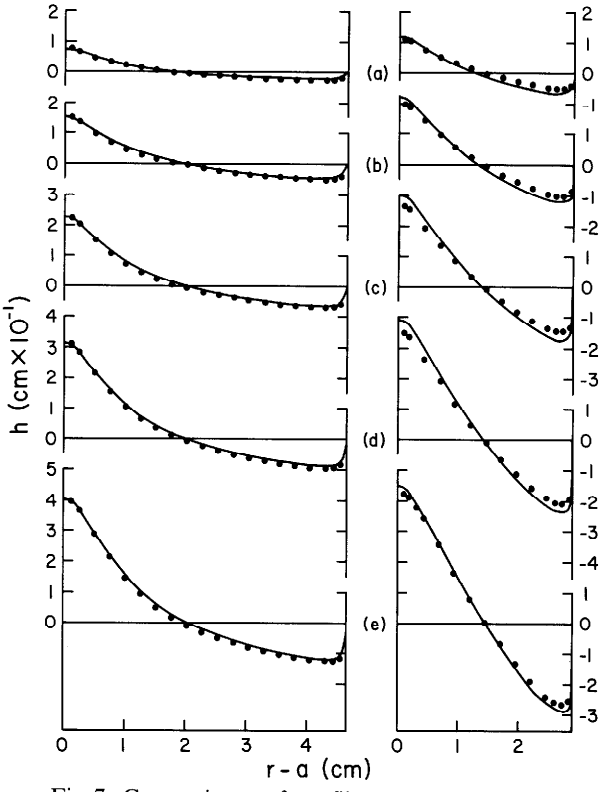

Fig. 7. Comparisons of profiles on TLA-227 for the smallest (3.936 cm) and largest (6.477 cm radius) inner cylinders when the inner cylinder is rotated clockwise (———) and counterclockwise (····)

gap was a difference in fluid temperature of between 1 °C and 2 °C for the two sets of measurements.

3.3. Experiments with STP

The free surface on a viscoelastic fluid with a much smaller valuc of the climbing constant than that of TLA-227 can assume an interesting variety of shapes which are very sensitive to the radii of the cylinders. Predicted free surface shapes for the sample of STP used in the present experiments are shown in figure 8 for several values of the inner cylinder radius. A rotational speed of 1.0 rev s^{-1} was used to construct the profiles, which are shown for two values of the climbing constant; $\hat{\beta} = 0.9$ and 0.5. These two values correspond to temperatures of 21 °C and 26 °C respectively, and were determined from the rotating rod data shown in the upper half of figure 4. The profiles of figure 8 emphasize the influence that small changes in temperature can have on the shape of the free surface. The two values of $\hat{\beta}$ used for figure 8 correspond to a temperature change of about 5 °C, and it is clear from these results that changes in temperature of only 1 °C could have a marked effect on the free surface shape.

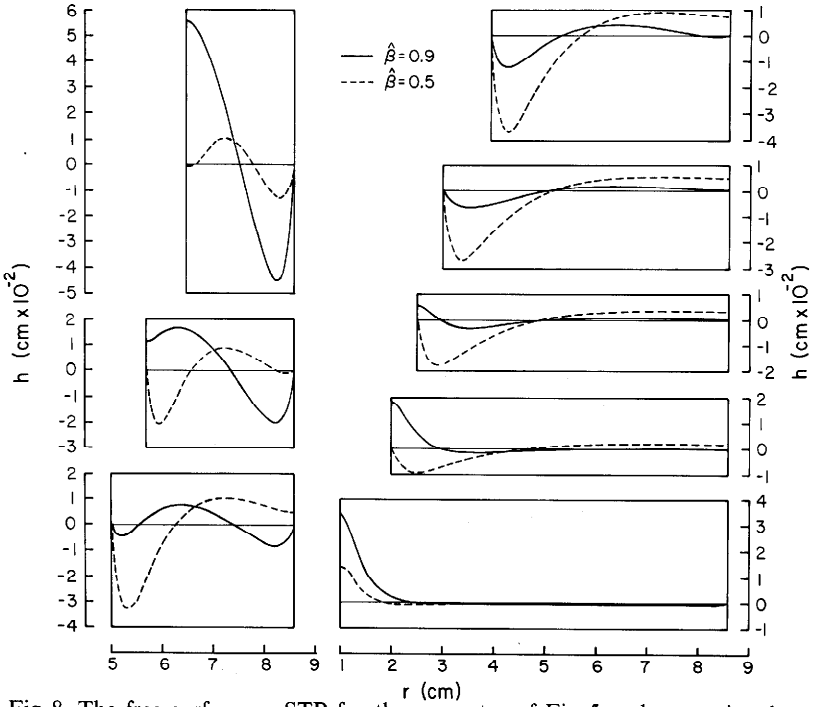

Fig. 8. The free surface on STP for the geometry of Fig. 5 and a rotational speed of 1.00 rev s^{-1}. Profiles for $\hat{\beta} = 0.9$ and 0.5 are given. The maximum climb is not always at the inner cylinder

Experimentally-measured profiles are compared with predicted profiles in figure 9. The calculations were performed with $\rho = 0.89$ gram cm^{-3}, $T = 30.7$ dynes cm^{-1} and a value of $\hat{\beta}$ corresponding to the actual fluid temperature for each experimental traverse across the surface. For this series of experiments the fluid temperature varied between 21.5 °C and 26.0 °C, and thus to get a realistic value for $\hat{\beta}$ for each run we used a simple linear interpolation between the values derived from the data of figure 4. The agreement between measured and predicted profiles at the lowest rotational speeds is again good, except for the largest inner cylinder (smallest gap size) where the lowest rotational speed may already be beyond the region of applicability of the second-order theory (see § 3.5). We attribute some of the smaller discrepancies between measured and predicted profiles at the lower rotational rates to possible non-uniformities in the fluid temperature. We can infer from figure 4 that the second-order region extends to higher rotational speeds for STP than it does for TLA-227, and we found it necessary to run at higher rotational speeds in order to produce measurable displacements. The higher rotational speeds lead to small perturbations in fluid temperature. We think, however, that the comparisons illustrated in figures 6 and 9 support the validity of the theoretical predictions at second order, and encourage confidence in the results obtained through order four for the determination of other viscoelastic parameters. Unfortunately, the calculations and experimental procedures required at fourth order are much more elaborate than those at second order and the higher order theory does not presently seem well suited for rheometrical measurements.

3.4. Experiments with polyacrylamide

The third part of our experimental program was conducted with a 2% solution of polyacrylamide in a glycerin-water mixture. The final results with this fluid did not exhibit the same level of agreement as that obtained with the other two fluids.

The value of the climbing constant could not be obtained with the same accuracy as for STP and TLA-227. We made several measurements at 24 °C (fig. 10) and obtained values between 1.10 and 1.21 gram cm^{-1}, with an average value of 1.15 gram cm^{-1}. When measuring the climbing constant with a rotating rod we usually coat the rod with Scotchgard, which gives a perpendicular contact of the fluid at the rod. This has no

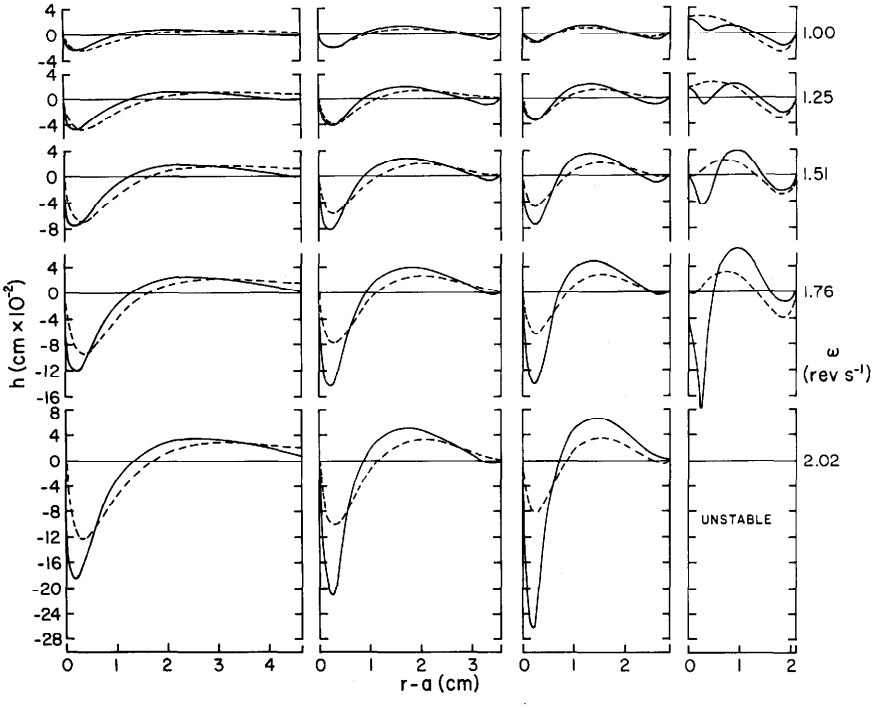

Fig. 9. Experimental (———) and predicted (– – –) profiles for STP for the experimental geometries of Fig. 6

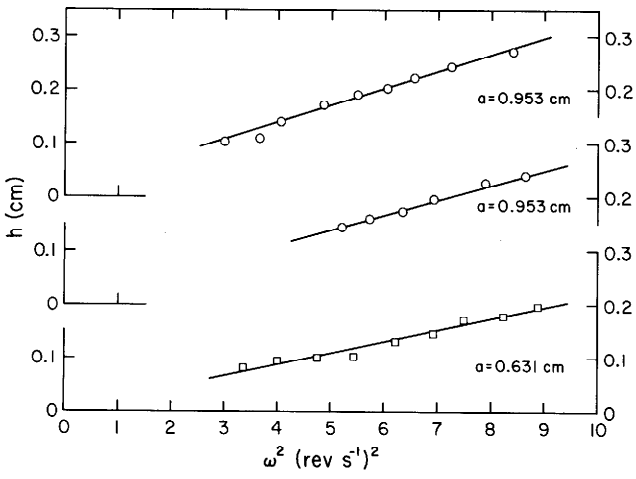

Fig. 10. The data from which the climbing constant for a 2% solution of polyacrylamide in 49% glycerin – 49% water was determined. The fluid temperature was 24 °C

effect on the climbing of STP and TLA-227 and other similar fluids we have used in experiments, but we did observe with polyacrylamide that at very low rotational speeds the fluid did not advance uniformly on the rod. This may account for the greater degree of scatter in the polyacrylamide data shown in figure 10, as compared with the data for STP and TLA-227 shown in figure 4.

All experimentally-measured profiles in the concentric cylinder apparatus were obtained with the fluid temperature between 24 °C and 25 °C. The profiles for counterclockwise rotation of the inner cylinder could not be distinguished

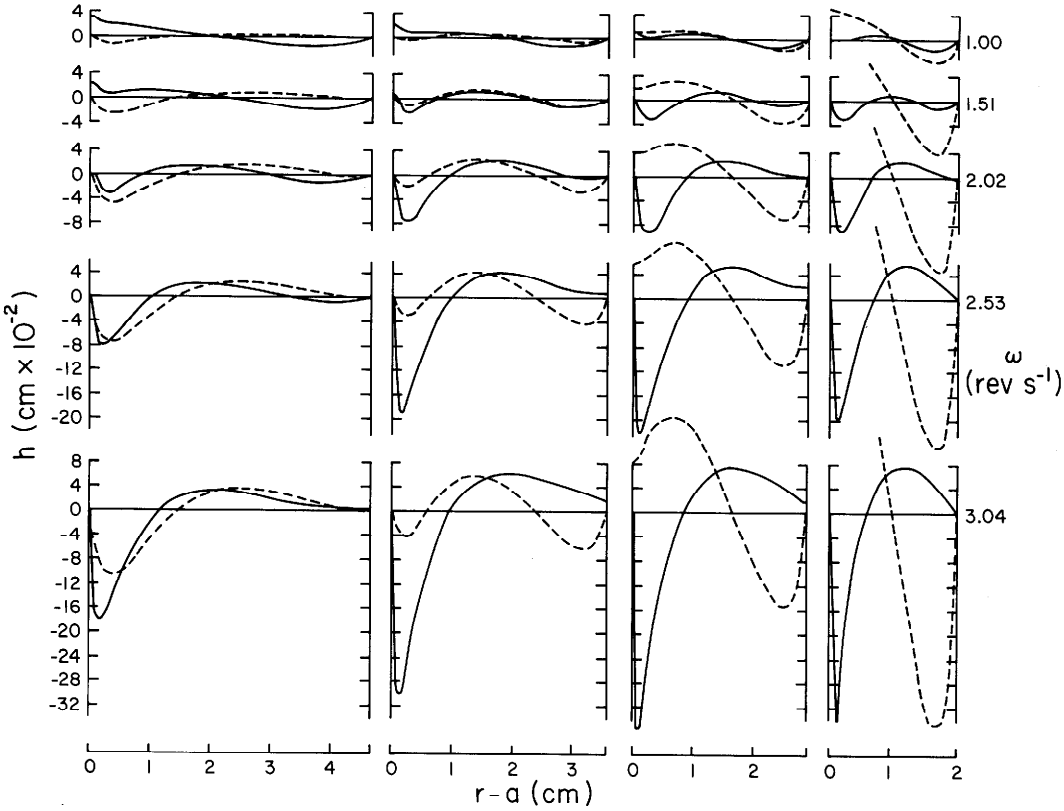

Fig. 11. Experimental (———) and predicted (– – –) profiles for a 2% solution of polyacrylamide in glycerin-water for the experimental geometries of Fig. 6

from the corresponding profiles for clockwise rotation. The measured profiles are shown in figure 11, and compared with predicted profiles which were computed using the following values for material parameters: $\hat{\beta} = 1.15$ gram cm^{-1}, $\rho = 1.128$ gram cm^{-3}, $T = 62$ dynes cm^{-1}.

There appears to be very little agreement between measured profiles and those predicted from second-order theory. In an attempt to find an explanation for this discrepancy we considered the possibility that we were using wrong values for $\hat{\beta}$ or T. We recalculated the profiles using values of 30 and 90 dynes cm^{-1} for the surface tension, with corresponding values of 1.0 and 1.25 gram cm^{-1} for $\hat{\beta}$. These calculations showed that surface tension has only a minor effect on the shape of the free surface. We then tried several values for $\hat{\beta}$ between 0.2 and 2.0 gram cm^{-1}, but found that the agreement was no better than (and usually was much worse than) that shown in figure 11.

Finally, since the measured values of $\hat{\beta}$ for STP and polyacrylamide are of the same order, we have compared experimentally-measured profiles on the two fluids at corresponding speeds (fig. 12). There are two obvious dissimilarities in the profiles on the two fluids. First the free surface deformations on STP are much greater than those on polyacrylamide, particularly at the higher rotational speeds. And second, polyacrylamide exhibits a climb up the inner cylinder at low rotational speeds and a depression near the inner cylinder at higher rotational speeds, whereas STP is depressed near the inner cylinder for all cylinders and at all speeds with the single exception of the largest inner cylinder rotating at 1.00 rev s^{-1}. We discuss some possible reasons for these differences in § 3.5 below.

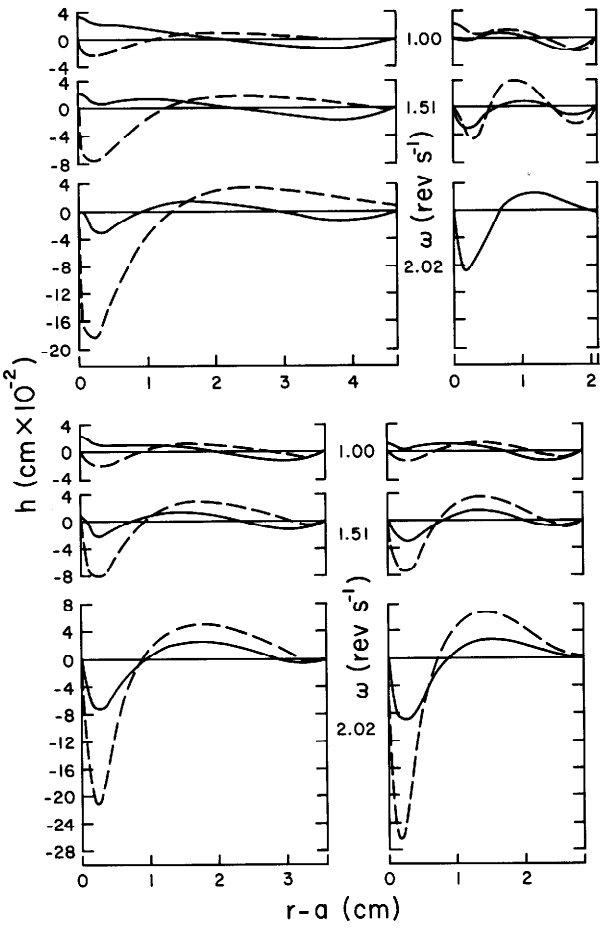

Fig. 12. Comparison of experimentally-measured profiles on STP and polyacrylamide at rotational speeds of 1.00, 1.51 and 2.02 rev s^{-1}

3.5. Discussion of results

The good agreement at low rotation speeds between the measured profiles on STP and TLA-227 and the corresponding profiles predicted from second-order theory using the value of the climbing constant $\hat{\beta}$ determined from rotating rods adds to our earlier work (4). In the earlier work we used rod experiments to determine reliable values for the climbing constants for oil-based fluids like STP. In those experiments and in these we were able to determine an apparent value for $\hat{\beta}$ for polyacrylamide in glycerin-water, but the fluid is unlike the oil-based ones and the experimental checks we use to test reliability are not so well satisfied in experiments using polyacrylamide.

The region of applicability of the second-order theory in the concentric cylinder geometry is different for different cylinder sizes and radius ratios. For the rotating rod viscometer we established (2) an ad hoc criterion to estimate the range of angular velocities for which the second-order theory may be expected to be valid. We adopt the same approach for concentric cylinders, and observe that the expansion for $h(r)$ can be expressed in terms of a modified Froude number $Fr = \Omega^2 l/g$, where l is a characteristic length depending on the apparatus and the fluid. This characteristic length is taken to be $0(h^{[2]}_{\max}(r)g)^{1/2}$, where $h^{[2]}_{\max}(r)$ is the distance between the highest and lowest points in the free-surface of the fluid. Asymptotic

Table 1

a (cm)	$0.28\,[h^{[2]}_{max}(r)]^{-1/4}$ rev s^{-1}		
	TLA-227 ($\hat{\beta} = 29.0$ gram cm^{-1})	STP ($\hat{\beta} = 0.6$ gram cm^{-1})	Polyacrylamide ($\hat{\beta} = 1.15$ gram cm^{-1})
3.936	0.45	1.34	1.68
5.018	0.42	1.38	1.74
5.704	0.40	1.56	1.41
6.477	0.37	1.36	1.09

validity for these series is expected when $Fr \ll 1$; our working criterion here is that second-order theory is valid when $Fr < 0.1$. This requirement gives

$$\omega^2 < \frac{0.1}{4\pi^2}\left[\frac{g}{h^{[2]}_{max}(r)}\right]^{1/2} (\text{rev s}^{-1})^2,$$

$$\omega < 0.28\,[h^{[2]}_{max}(r)]^{-1/4} \text{ rev s}^{-1}.$$

From the numerical solution used to construct figures 6, 9 and 11 we have computed the estimates shown in table 1 for the limits of applicability of the second-order theory.

In general, as the gap between the cylinders gets smaller, the terms of order higher than second begin to be important at lower rotational speeds. These results are not inconsistent with our observations, and suggest that, with the largest inner cylinder in the apparatus, the lowest speed at which we could measure a free surface deformation on STP and polyacrylamide might be too large for second-order theory to be valid.

We are not able to give a satisfactory explanation of why the theory, which works well for STP and TLA-227, does not appear to work for polyacrylamide. We can speculate, however, that the reason is related to material properties of the polyacrylamide solution. One (not so likely) possibility is that the dynamics of the free surface is not governed by the classical theory of surface tension. For example, eq. [9] for $h^{[2]}$ is derived from [4] which equates the jump in the normal stress across the free surface to the surface tension force. The constitutive relations of the classical theory of surface tension have been assumed in writing [4], and as we noted in our work with the rotating rod viscometer (4), classical surface tension may be inadequate to explain surface behavior at an air-polyacrylamide interface. The response of the polyacrylamide surface to a ring tensiometer is viscoelastic and unlike that of a Newtonian fluid. When the ring is pulled out of the surface, the film of polyacrylamide which attaches to the ring slowly stretches to several times the height that it would for a pure glycerin-water solution before the breaking process begins. Unlike the film of a Newtonian fluid which ruptures very suddenly, the sheet of polyacrylamide supported by the ring slowly collapses on to the ring, so that a configuration is reached consisting of a membrane of fluid stretched across the ring with a small jet of fluid draining from the center of the membrane into the main body of fluid. As the fluid continues to drain out of the membrane it eventually causes the membrane to rupture. TLA-227 behaves in a similar manner, so it is unlikely that this is the sole reason for the discrepancy.

We have observed that polyacrylamide solutions tend to form a skin on the surface when left exposed to the atmosphere, but this has no apparent influence on the value of the surface tension. In any case, as we have noted earlier, even large changes in the value of the surface tension produce only small changes in the computed free-surface profiles.

Another factor which may be significant is that both STP and TLA-227 have a nearly Newtonian shear stress, whereas polyacrylamide is quite pseudoplastic (6, 7). For example, *Boger's* experiments (6) with a 0.4% polyacrylamide solution show a pseudoplastic behavior over almost six decades of shear rate. *Boger* and *Cable* (8) have also observed an unusual behavior in the first normal-stress difference for polyacrylamide solutions (Separan AP 30 and MG 500). For several different concentrations they report a discontinuity in the first normal-stress difference data while the shear stress remains continuous. The discontinuities occurred in the shear rate range of 7 to 250 s^{-1}, which are of the same order as the shear rates

in our experiments. They were unable to find an adequate explanation for the discontinuities, and concluded: "We are then left with the proposition that a structural change is occurring in a shear field for these materials".

Acknowledgement

This work was supported by the U.S. Army Research Office.

Summary

This paper is a further contribution to our work on the Weissenberg effect. One goal of our work is to show how the free-surface deformations on a viscoelastic fluid which is sheared between two concentric rotating cylinders can be used to determine rheological data about the fluid. In this paper we report the results of an experimental program in which free surface shapes have been measured on three viscoelastic fluids undergoing shearing in an apparatus consisting of a stationary outer cylinder and four interchangeable rotating inner cylinders. Experimentally-measured profiles are compared with profiles predicted from second-order theory, and found to be in excellent agreement for STP and TLA-227 in the range of applicability of the second-order theory, but there is some disagreement in the results for a 2% solution of polyacrylamide in 49% water – 49% glycerin.

Zusammenfassung

Diese Arbeit stellt einen weiteren Beitrag zu unseren Untersuchungen über den Weissenberg-Effekt dar. Ein Ziel dieser Untersuchungen ist es zu zeigen, wie die Deformation der freien Oberfläche einer zwischen zwei konzentrischen Zylindern gescherten viskoelastischen Flüssigkeit dazu verwendet werden kann, rheologische Kenngrößen der Flüssigkeit zu gewinnen. In dieser Arbeit wird über die Ergebnisse einer experimentellen Untersuchung berichtet, in der die Gestalt der freien Oberfläche bei drei viskoelastischen Flüssigkeiten gemessen wurde, die in einem Apparat geschert wurden, der aus einem stationären Außenzylinder und vier auswechselbaren rotierenden Innenzylindern bestand. Die experimentell bestimmten Profile werden mit solchen verglichen, die aufgrund einer Theorie zweiter Ordnung vorausgesagt worden sind. Man findet im Bereich der Anwendbarkeit dieser Theorie für STP und TLA-227 eine ausgezeichnete Übereinstimmung, wohingegen die Ergebnisse bei einer 2%igen Polyacrylamid-Lösung in einer 1 : 1-Wasser-Glycerin-Mischung gewisse Diskrepanzen aufweisen.

References

1) *Joseph, D. D., G. S. Beavers*, Rheol. Acta **16**, 169 (1977).

2) *Joseph, D. D., R. L. Fosdick*, Arch. Rational Mech. Anal. **49**, 321 (1973).

3) *Joseph, D. D., G. S. Beavers, R. L. Fosdick*, Arch. Rational Mech. Anal. **49**, 381 (1973).

4) *Beavers, G. S., D. D. Joseph*, J. Fluid Mech. **69**, 475 (1975).

5) *Yoo, J., D. D. Joseph, G. S. Beavers*, J. Fluid Mech. **92**, 529 (1979).

6) *Boger, D. V.*, Nature **265**, 126 (1977).

7) *Good, P. A., A. J. Schwartz, C. W. Macosko*, Amer. Inst. Chem. Engs. J. **20**, 67 (1974).

8) *Boger, D. V., P. J. Cable*, Rheol. Acta **16**, 322 (1977).

Authors' addresses:

Prof. *G. S. Beavers*, Prof. *D. D. Joseph*
Department of Aerospace Engineering and Mechanics
University of Minnesota
107 Aeronautical Engineering Building
110 Union Street S.E.
Minneapolis, Minnesota 55455 (USA)

Dr. *J. Y. Yoo*
Department of Mechanical Engineering
Seoul National University
Seoul (Korea)